CO_2 and HCN in the circumstellar envelopes of the low mass-loss rate AGB stars R Leo and Y CVn

José Pablo Fonfría

jpablo.fonfria@csic.es

Instituto de Física Fundamental (IFF)
Consejo Superior de Investigaciones Científicas (CSIC)

with the collaboration of

E. J. Montiel, J. Cernicharo, C. N. DeWitt, M. J. Richter, J. H. Lacy, T. K. Greathouse, M. Santander-García, M. Agúndez & S. Massalkhi

SOFIA Tele-Talk

July 7, 2021

Outline

Introduction

Typical AGB stars:

- Masses: $0.5 - 8.0\ \mathrm{M}_\odot$ (Gautschy & Saio 1996)
- Pulsation periods: $80 - 800$ d (Gautschy & Saio 1996)
- $10^{-7} \lesssim \dot{M}(\mathrm{M}_\odot\ \mathrm{yr}^{-1}) \lesssim 10^{-5}$ (Loup et al. 1993; De Beck et al. 2010; Ramstedt et al. 2014,2020)
- Terminal gas expansion velocity $\simeq 5 - 25$ km s^{-1} (Danilovich et al. 2015; Ramstedt et al. 2020)
- $T_{\mathrm{eff}} \lesssim 3500$ K (Bergeat et al. 2001)
- Dust grains made of (Agúndez et al. 2020):
  - C-type stars (C/O > 1): amorphous carbon+SiC+$\cdots$
  - M-type stars (C/O < 1): silicates+Al_2O_3+$\cdots$
  - S-type stars (C/O $\simeq 1$): MgS+silicates+Al_2O_3+$\cdots$
- Gas-to-dust ratio: $10 - 10\,000$ ($\simeq 300$ in average) (Massalkhi et al. 2018, 2020)

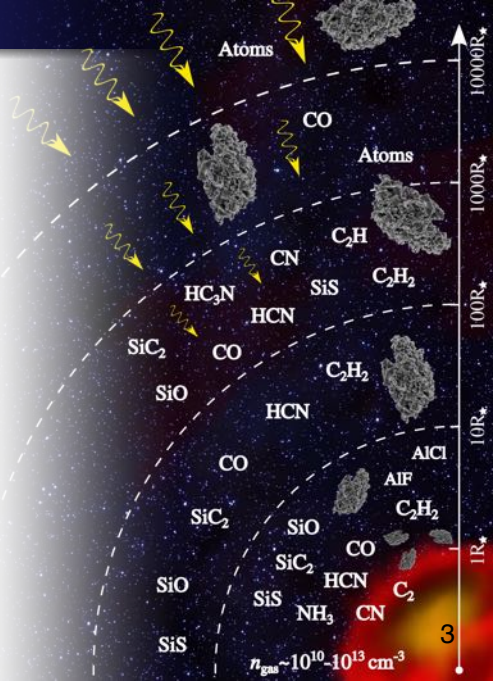

Introduction

Circumstellar chemistry:

- High mass-loss rate stars:
  1. Parent molecules (CO, HCN, C_2H_2, SiS, SiC_2,...) formed close to the star
  2. Dust grains form from refractory molecules
  3. Parent molecules reach the outer envelope
  4. Parent molecules dissociated into radicals
  5. Active chemistry $\Longrightarrow$ Many new molecules
- Low mass-loss rate stars:
  - The outer layers move inwards by a factor of $\simeq 10$ compared to high mass-loss rate stars $\Longrightarrow$ higher density and temperature
  - Different molecular abundances and new species?
- How does the evolution of the envelope depend on the chemistry in the vicinity of the star?
- How do the matter ejection mechanisms affect the chemistry close to the star?

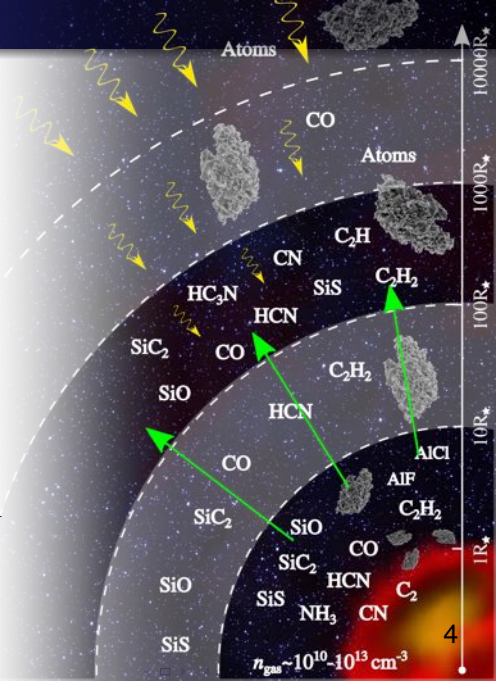

Introduction: Vibrational structure of a molecule

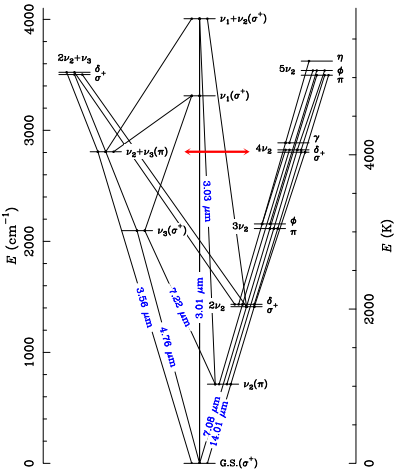

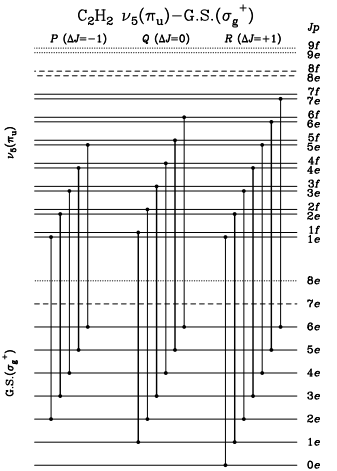

Vibrational energy pattern of HCN below 6000 K (left) typical transitions in a ro-vibrational band of C_2H_2 (right). (left) The lines connecting states represent allowed vibrational transitions. The wavelengths at which several of the transitions occur are indicated in blue. (right) The thick and thin levels are affected by spin statistics (ortho-para) with a ratio of 3:1. The vertical lines represent the allowed transitions.

Introduction: Low spectral resolution spectroscopy

- Very sensitive observations thanks to the low spectral resolution ($R = \lambda/\delta\lambda \sim 100 - 1000$). The SED of faint objects can be accurately described (e.g., JWST)
- Solid state bands (or their lack) are noticeable (mineralogy)
- Detection of bands of abundant molecular species (CO, C_2H_2, HCN, H_2O, CO_2, SiO,...) is common
- New molecules (usually with low abundance) can be detected as well

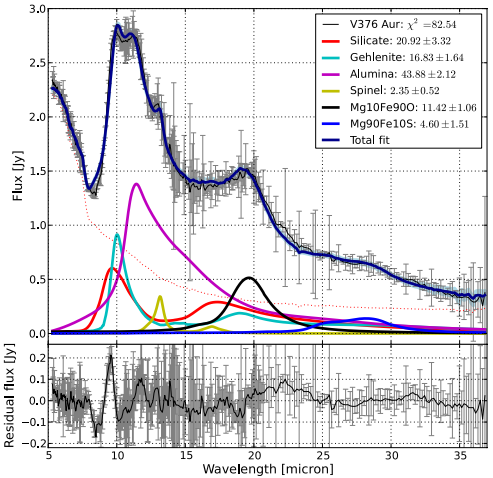

Spitzer observations of the S-type star V376 Aur and the best fit to its SED (Smolders et al., 2012,, A&A, 540, A72)

Introduction: Low spectral resolution spectroscopy

- Very sensitive observations thanks to the low spectral resolution ($R = \lambda/\delta\lambda \sim 100 - 1000$). The SED of faint objects can be accurately described (e.g., JWST)
- Solid state bands (or their lack) are noticeable (mineralogy)
- Detection of bands of abundant molecular species (CO, C_2H_2, HCN, H_2O, CO_2, SiO,...) is common
- New molecules (usually with low abundance) can be detected as well

Refs.: Markwick & Millar, 2000, A&A, 359, 1162; Molster et al., 2001, A&A, 366, 923; Sloan et al., 2010, ApJ, 719, 1274; Baylis-Aguirre et al., 2020, MNRAS, 493, 807;...

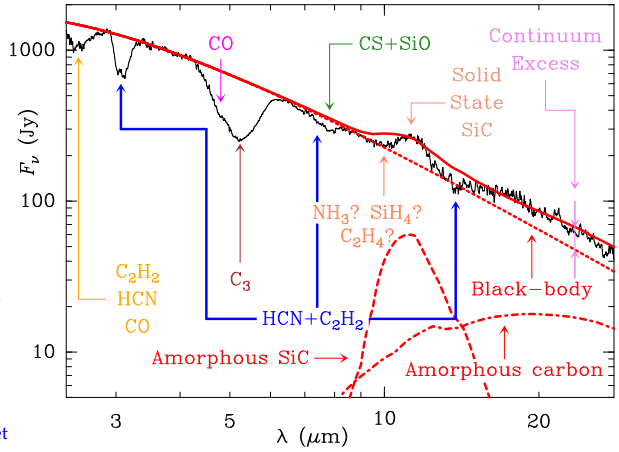

Spectral energy distribution of the J-type star Y CVn in the spectral range $\simeq 2.5 - 30$ μm. The main contributions to the continuum emission have been separated. The carriers of the molecular bands are identified (Yang et al., 2004, A&A, 414, 1049; Fonfría et al., submitted to A&A)

Introduction: Low spectral resolution spectroscopy

- Very sensitive observations thanks to the low spectral resolution ($R = \lambda/\delta\lambda \sim 100 - 1000$). The SED of faint objects can be accurately described (e.g., JWST)
- Solid state bands (or their lack) are noticeable (mineralogy)
- Detection of bands of abundant molecular species (CO, C_2H_2, HCN, H_2O, CO_2, SiO,...) is common
- New molecules (usually with low abundance) can be detected as well

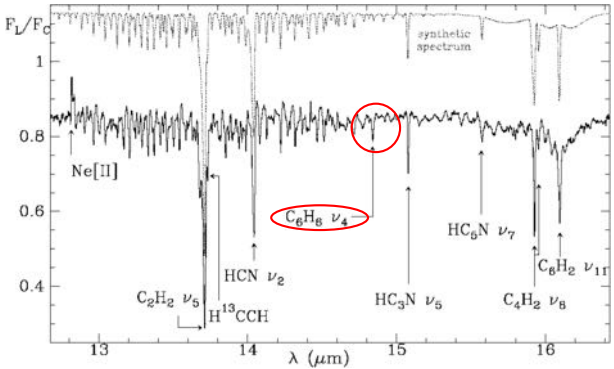

First detection of benzene (among other molecules and one atom) in the 12.7—16.5 μm *spectral range of the ISO/SWS observations of the PPN CRL618 (Cernicharo et al., 2001, ApJ, 546, L123)*

Introduction: Low spectral resolution spectroscopy

- Very sensitive observations thanks to the low spectral resolution ($R = \lambda/\delta\lambda \sim 100 - 1000$). The SED of faint objects can be accurately described (e.g., JWST)
- Solid state bands (or their lack) are noticeable (mineralogy)
- Detection of bands of abundant molecular species (CO, C_2H_2, HCN, H_2O, CO_2, SiO,...) is common
- New molecules (usually with low abundance) can be detected as well

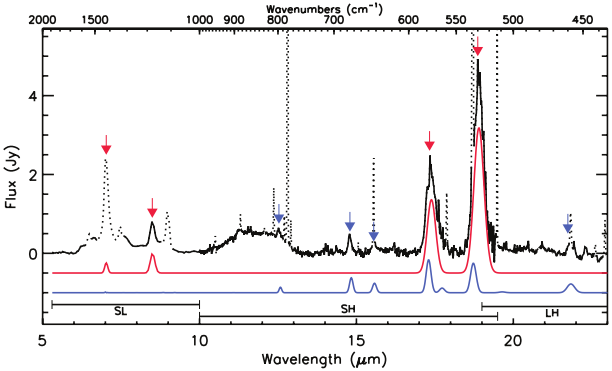

First detection of C_{60} and C_{70} in Spitzer observations of the young PN Tc1 (Cami et al., 2010, Science, 329, 1180)

Introduction: Low spectral resolution spectroscopy

- Very sensitive observations thanks to the low spectral resolution ($R = \lambda/\delta\lambda \sim 100 - 1000$). The SED of faint objects can be accurately described (e.g., JWST)
- Solid state bands (or their lack) are noticeable (mineralogy)
- Detection of bands of abundant molecular species (CO, C_2H_2, HCN, H_2O, CO_2, SiO,...) is common
- New molecules (usually with low abundance) can be detected as well

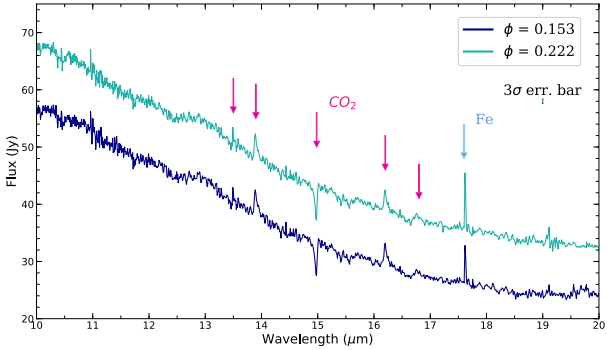

Vibrational spectrum of CO_2 in Spitzer observations of R Tri (Baylis-Aguirre et al., 2020, MNRAS, 493, 807). Similar observations were taken with ISO toward EP Aqr (Cami et al., 2000, A&A, 360, 562) among many others

Introduction: High spectral resolution spectroscopy

C_3 and C_5 in IRC+10216

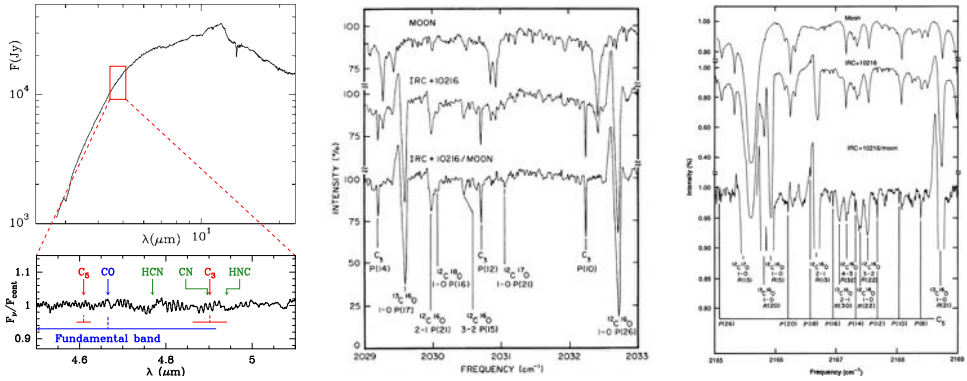

First detections of C_3 (middle) and C_5 (right) in IRC+10216. The low spectral resolution observation taken with ISO/SWS (left) shows no evidence of the spectra of these molecules, mainly because the CO spectrum dominates the spectral range, hiding the C_3 and C_5 lines (Hinkle et al. 1988; Bernath et al. 1989; Cernicharo et al. 1999)

Introduction: High spectral resolution spectroscopy

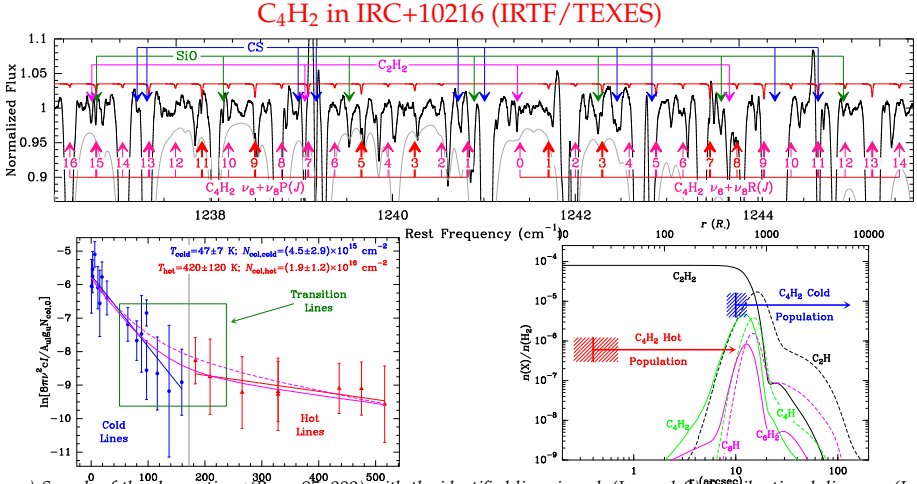

(Upper) Sample of the observations ($R \simeq 85,000$) with the identified lines in red. (Lower left) Ro-vibrational diagram. (Lower right) Chemical model with the observational constraints (Fonfría et al., 2018)

Introduction: Gas kinematics and molecular excitation

- Low spectral resolution observations cannot be used to derive accurate conclusions about the gas kinematics
- High spectral resolution observations are useful to:
  - Derive kinematic information about the gas expansion velocity profile over the gas acceleration zone
  - Study the gas turbulence close to the star
  - Determine the excitation temperatures (rotational and vibrational) throughout the envelope
  - Find asymmetries in the latter quantities along the line-of-sight

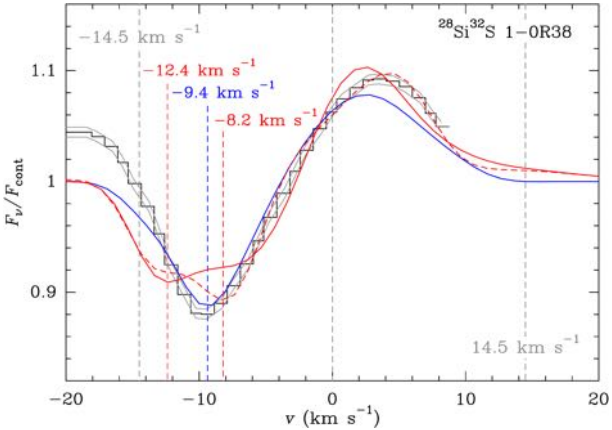

SiS 1-0R(38) line toward the carbon rich star IRC+10216, observed with the TEXES spectrograph mounted on the IRTF ($R \simeq 75\,000$; black). The solid red, dashed red, and solid blue curves are models calculated by assuming different gas expansion velocity profiles (Fonfría et al. 2015).

Introduction: Gas kinematics and molecular excitation

- Resolved ro-vibrational bands contains many lines involving levels with different energies that are excited in different regions of the envelope.
- The use of many lines of fundamental and hot bands is useful to trace the whole envelope paying a special attention to the inner layers.
- All these lines can be observed simultaneously in less than 1 hour of observing time.
- The opacities of all the lines are blended in unresolved vibrational bands.

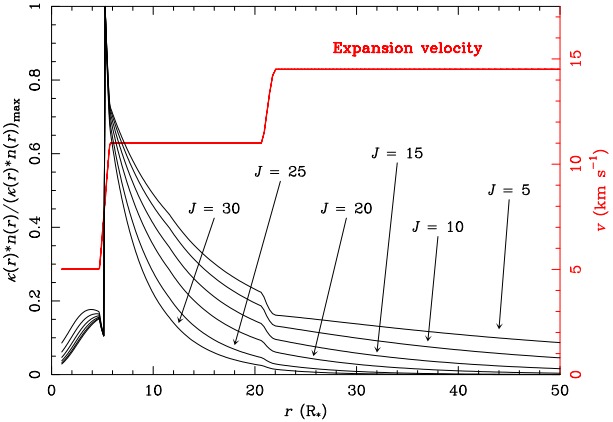

Opacity of several C_2H_2 lines of the fundamental band $\nu_5(\pi_u)$ for IRC+10216 and the assumed gas expansion velocity. Each opacity is normalized at its maximum to allow for a direct comparison (Fonfría et al. 2008).

Mid-IR survey of AGB stars (SOFIA/EXES)

- Survey of AGB stars with different mass-loss rates ($\sim 10^{-7} - 10^{-5}$ $M_\odot$ yr^{-1}) and chemistry types (C, S, O) carried out with SOFIA/EXES (program 06_0144, PI: E. J. Montiel).
- Stars observed so far:
  - C-rich: IRC+10216, Y CVn
  - S-type: χ Cyg, W Aql
  - O-rich: VX Sgr, IK Tau, R Leo
- Characteristics of the observed spectra:
  - Several settings at $\simeq$ 13.5 μm and 7.5 μm
  - High_Low mode when possible, otherwise High_Medium mode
  - Maximum frequency coverage: $702 - 783$ cm^{-1} ($12.77 - 14.24$ μm), $1312 - 1358$ cm^{-1} ($7.36 - 7.62$ μm)
  - Resolving power (R) ranging from 60,000 to 85,000 (spectral resolution of $3.5 - 5.0$ km s^{-1})
  - S/N $\gtrsim$ 100 (with respect to the continuum)
  - Telluric calibrators: Ceres, Vesta. Atmospheric transmission model: ATRAN

Mid-IR survey of AGB stars (SOFIA/EXES)

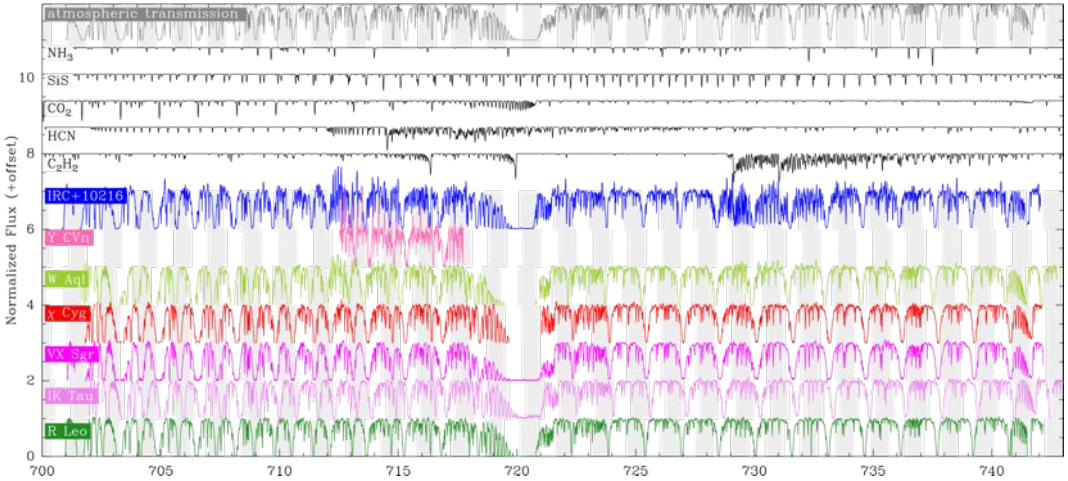

Overview of the data around 13.8 μm *taken under the frame of the SOFIA program 06_0144 (P.I.: E. J. Montiel) (Montiel et al., in preparation; Fonfría et al., in preparation).*

Mid-IR survey of AGB stars (SOFIA/EXES)

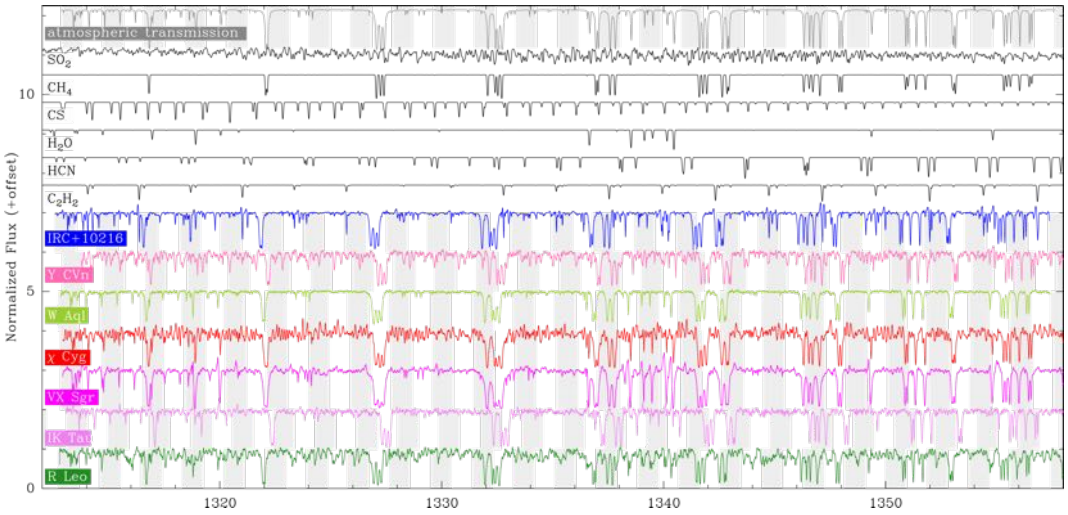

Overview of the data around 13.8 μm *taken under the frame of the SOFIA program 06_0144 (P.I.: E. J. Montiel) (Montiel et al., in preparation; Fonfría et al., in preparation).*

Molecules potentially detectable in our survey

Molecule	Stars						
	C-rich		S-type		O-rich		
	IRC+10216	Y CVn	W Aql	χ Cyg	VX Sgr	IK Tau	R Leo
C_2H_2	✔	✔	✔	✘			✘
CH_4							
CS	✔	✔	✘				
SiS	✔	✘					
HCN	✔	✔	✔	✘			
NH_3							
SO_2	✘	✘		✔		✔	✔
H_2O					✔	✔	✔

Notes.- ✔*: detected;* ✘*: undetected; blanks mean that the molecule has not been searched for or we are still not sure about its detection or undetection.*

CO_2 in the O-rich star R Leo

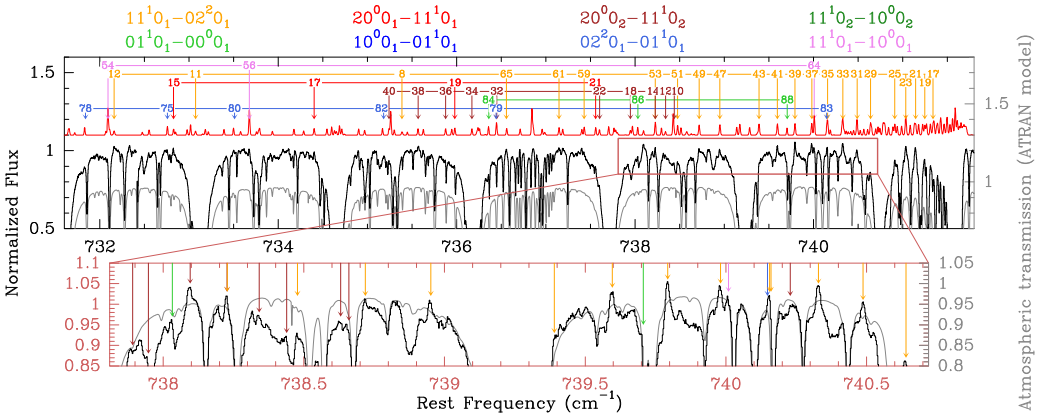

Part of the observed spectrum of R Leonis around $\simeq$ 13.6 μm (black). The gray spectrum is a model of the atmospheric transmission. The red spectrum is an approximate model of the CO_2 emission. The lower panel contains a zoom to an interesting part of the spectrum. We have indicated the CO_2 lines found in the observations. Each color corresponds to a band (involving the vibrational states $v_1 v_2^{\ell} v_{3,r}$) above the upper panel (Fonfría et al., 2020).

CO_2 in the O-rich star R Leo

- We found $\simeq$ 250 ro-vibrational CO_2 and $^{13}CO_2$ lines of 8 bands in emission *only* in the R Leo spectrum among the atmospheric CO_2 features. The Doppler shift is high enough to release the lines coming from the star.
- The CO_2 lines coming from R Leo are frequently Gaussian-like but not always.
- The emission comes from two regions of the envelope:
  - one at $\simeq 2.0 - 3.5 R_\star$ triggered by the stellar continuum at 2.7 and 4.2 μm, and
  - another at $\simeq 10 R_\star$ where the dust emission around 15 μm plays an important role

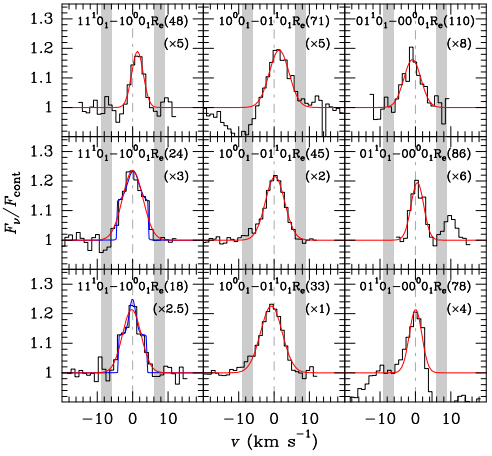

Sample of CO_2 after the baseline removal. These lines have been fitted with one Gaussian (red) or with one Gaussian and a rectangular profile (blue) (Fonfría et al., 2020).

CO_2 in the O-rich star R Leo

- We found $\simeq 250$ ro-vibrational CO_2 and $^{13}CO_2$ lines of 8 bands in emission *only* in the R Leo spectrum among the atmospheric CO_2 features. The Doppler shift is high enough to release the lines coming from the star.
- The CO_2 lines coming from R Leo are frequently Gaussian-like but not always.
- The emission comes from two regions of the envelope:
  - one at $\simeq 2.0 - 3.5 R_\star$ triggered by the stellar continuum at 2.7 and 4.2 μm, and
  - another at $\simeq 10 R_\star$ where the dust emission around 15 μm plays an important role

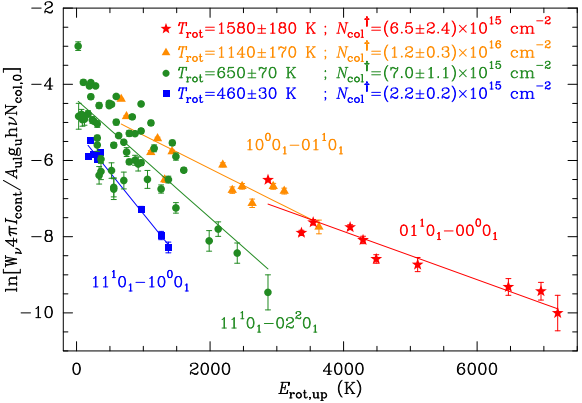

Ro-vibrational diagram of the lines of the strongest bands. Interestingly, the bands involving higher excitation vibrational states show lower rotational temperatures, which suggest a radiative vibrational excitation (Fonfría et al., 2020).

CO_2 in the O-rich star R Leo

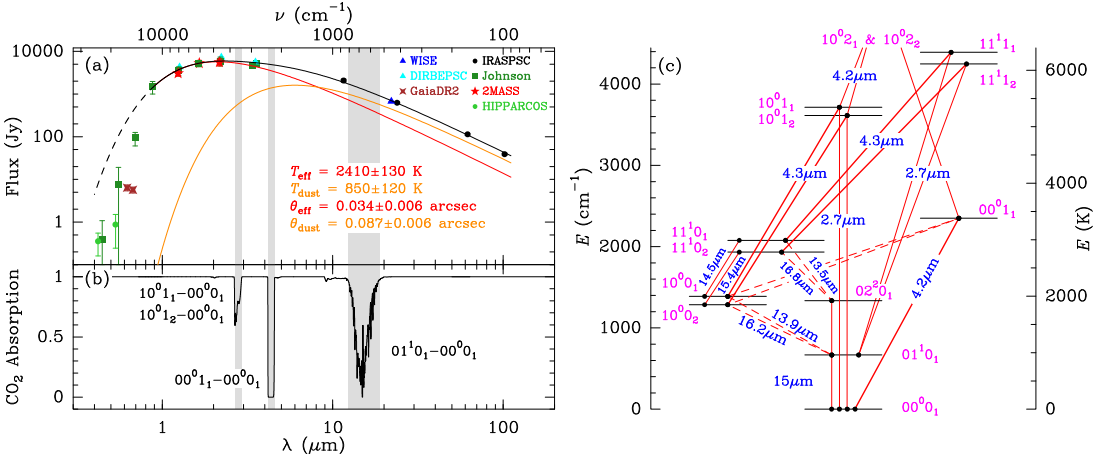

Effect of the continuum emission of R Leo on the vibrational excitation of CO_2. (a) Continuum emission derived from a fit to photometric measures. (b) Low spectral resolution absorption spectrum of CO_2. (c) CO_2 vibrational energy diagram below 6000 K. The absorption of stellar continuum at 2.7 and 4.2 μm is the responsible of the observed lines of the $10^00_1 - 01^10_1$ and $10^00_2 - 01^10_1$ bands. The enhancement of the population of the state 01^10_1 due to the dust emission at $10R_\star$ increases the intensity of lines of the $11^10_1 - 02^20_1$ and $11^10_2 - 02^20_1$ bands (Fonfría et al., 2020).

CO_2 in the O-rich star R Leo: Conclusions

- The spectrum of CO_2 is detected for first time in the O-rich AGB star R Leo.
- This detection was possible thanks to SOFIA's cruising altitude above 35 000 ft and the favorable Doppler shift that separates the lines coming from R Leo from the telluric features.
- Most of the lines, which are all of them in emission, shows Gaussian-like profiles. The rest of them display two components (Gaussian+square profiles).
- The ro-vibrational diagram reveals that there are three different thermal populations at temperatures of 1600, 1150, and 550 K. The responsible molecules are placed at 2.2, 3.5, and $10R_\star$.
- The observed lines are produced by fluorescence caused by absorption of the stellar continuum at 2.7 and 4.2 μm. Dust emission favors the formation of certain bands.
- The comparison between the column density we derived ($\simeq 7 \times 10^{17}$ cm^{-2}) and previous measures of other stars with CO_2 suggests that either the amount of CO_2 does not depend on the mass-loss rate or the column density needs to be better determined.
- Fonfría, Montiel, Cernicharo, DeWitt & Richter, 2020, A&A, 643, L15

HCN in the C-rich star Y CVn

- SOFIA/EXES
  - $712.5 - 717.7\ \mathrm{cm}^{-1}$ ($13.93 - 14.04\ \mu$m)
  - $1313.7 - 1358.2\ \mathrm{cm}^{-1}$ ($7.36 - 7.61\ \mu$m)
  - $R \simeq 67,000$@14 μm and $\simeq 60,000$@7.5 μm
  - HCN and $H^{13}CN$ detected lines:
- IRTF/TEXES
  - $754.7 - 769.2\ \mathrm{cm}^{-1}$ ($13.00 - 13.25\ \mu$m)
  - $R \simeq 83,000$
  - HCN and $H^{13}CN$ detected lines:
- IRAM/30m telescope
  - $88.6 - 267.2$ GHz ($1.12 - 3.38$ mm)
  - HCN and $H^{13}CN$ detected lines: 5
- ISO/SWS+LWS and several photometric catalogs
  - $100 - 10000\ \mathrm{cm}^{-1}$ ($1 - 100\ \mu$m)
  - $R \simeq 200 - 500$

HCN in the C-rich star Y CVn

SOFIA/EXES@14 μm

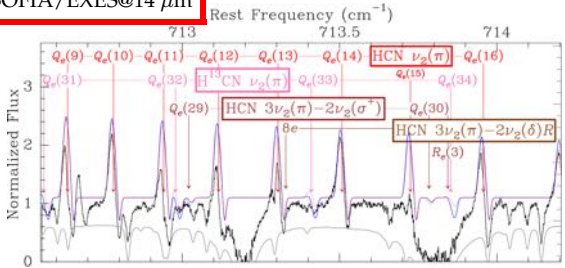

SOFIA/EXES@7.5 μm

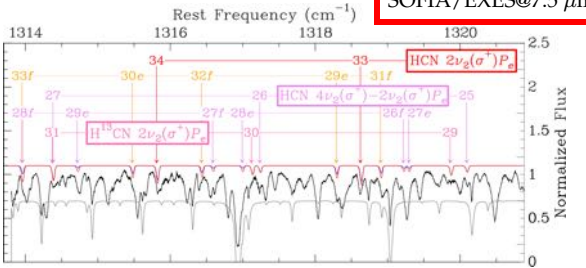

IRTF/TEXES@13.1 μm

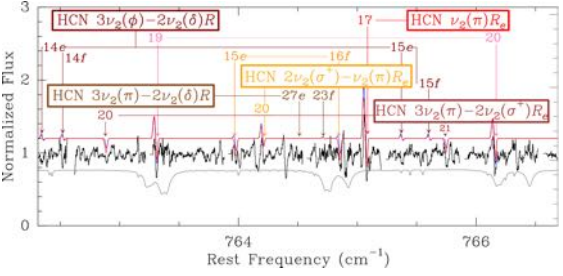

IRAM/30m@1.12 mm

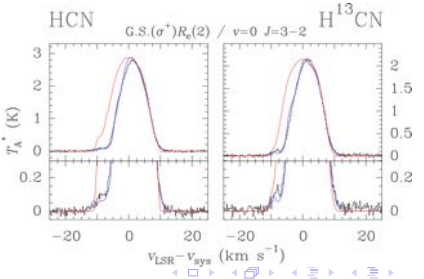

HCN in the C-rich star Y CVn: Continuum

The SED of Y CVn can be described by:

- A compact blackbody with an effective temperature of 2900 K
- Warm to hot SiC dust (band at 11.3 μm)
- Cold amorphous carbon (emission excess beyond $\simeq$ 15 μm)
- Several molecular bands produced by CO, C_3, C_2H_2, HCN, CS, and SiO
- A strong absorption at short wavelengths ($\simeq 1.0 - 1.5$ μm; not considered by the model) due to the C_2 and CN ro-vibronic bands (Phillips and Red systems, respectively)

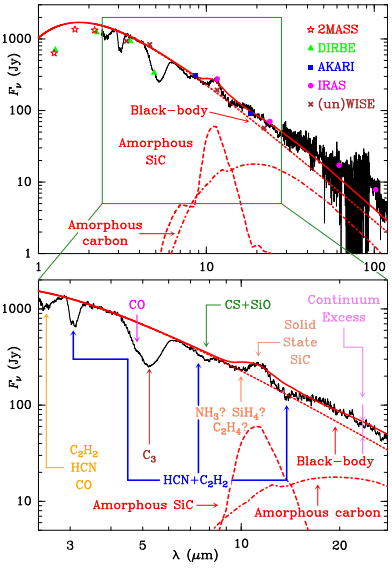

HCN in the C-rich star Y CVn: Ro-vibrational diagram of HCN

The ro-vibrational diagram based on the lines of the strongest bands shows:

- There are four thermal populations of HCN ($T_{\rm rot} \simeq 100$, 480, 1300, and 3300 K)
- The observed lines at 14.0 μm describe most of these populations
- The observed lines at 7.5 μm are more sensitive to high rotational temperatures
- There is a clear discrepancy between the column densities derived from the lines at 7.5 and 14.0 μm

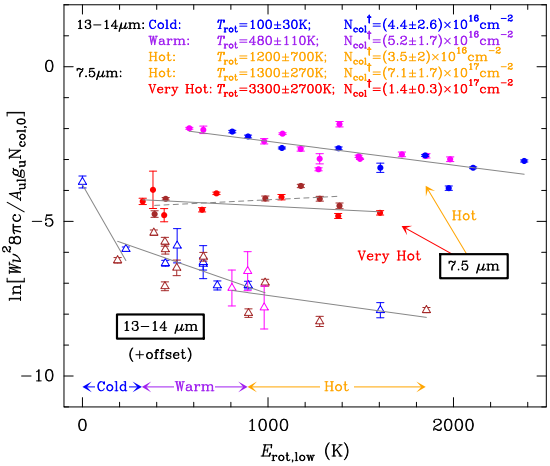

HCN in the C-rich star Y CVn: Detailed 1D modeling of HCN

A detailed modeling of all the observed spectra done with the radiation transfer code developed by Fonfría et al. (2008) and Fonfría et al. (2014) indicates that:

- It is not possible to simultaneously reproduce the lines observed at 14.0 μm and 7.5 μm with the same spherically symmetric envelope model
- The best envelope models for any of these data sets produce bad synthetic lines for the other.
- The rotational lines can be describe with the envelope model derived from the observations at 14.0 μm

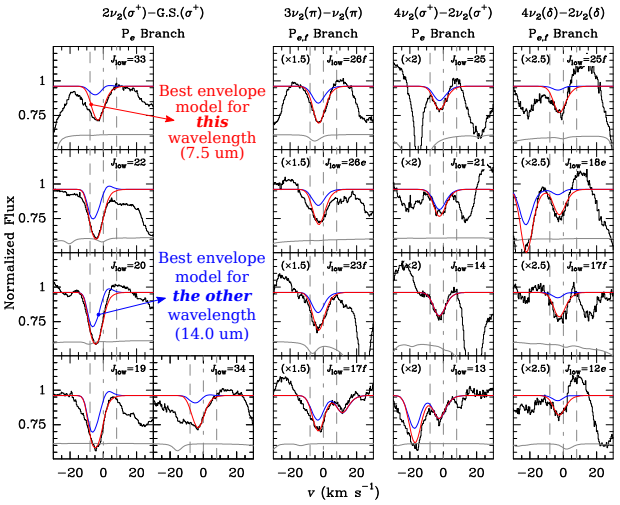

HCN in the C-rich star Y CVn: Line wings

- Three HCN lines of the fundamental band ν_2 with low-J at 14 μm display what seem to be red-shifted wings.
- Similar red-shifted wings might exist in the rest of the low-J lines but they are contaminated by telluric features and other HCN lines.
- The rotational lines of HCN and $H^{13}CN(v = 0; J = 3 - 2)$ also shows red-shifted wings.
- These wings cannot be explained by their hyperfine structure.
- The spherically symmetric models are not able to reproduce them.

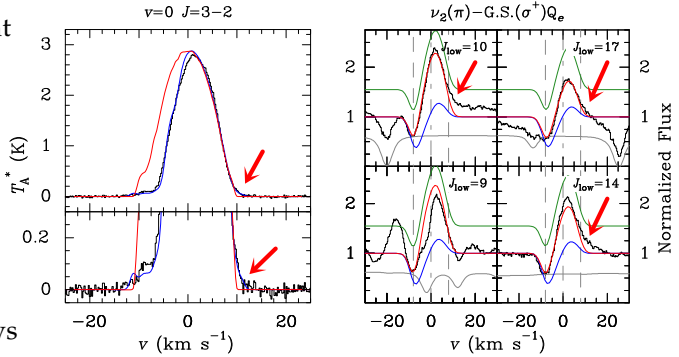

HCN lines (rotational to the left and ro-vibrational to the right) where we found red-shifted wings. (left) The red curve is the synthetic line calculated with the spherically symmetric envelope model. The blue curve is the synthetic line calculated with the 2D envelope model (see next slide). (right) The red and blue curves are the lines calculated with the spherically symmetric envelope models (as in the previous slide). The green curves are the lines calculated with the 2D envelope model.

HCN in the C-rich star Y CVn: Rough 2D modeling of HCN

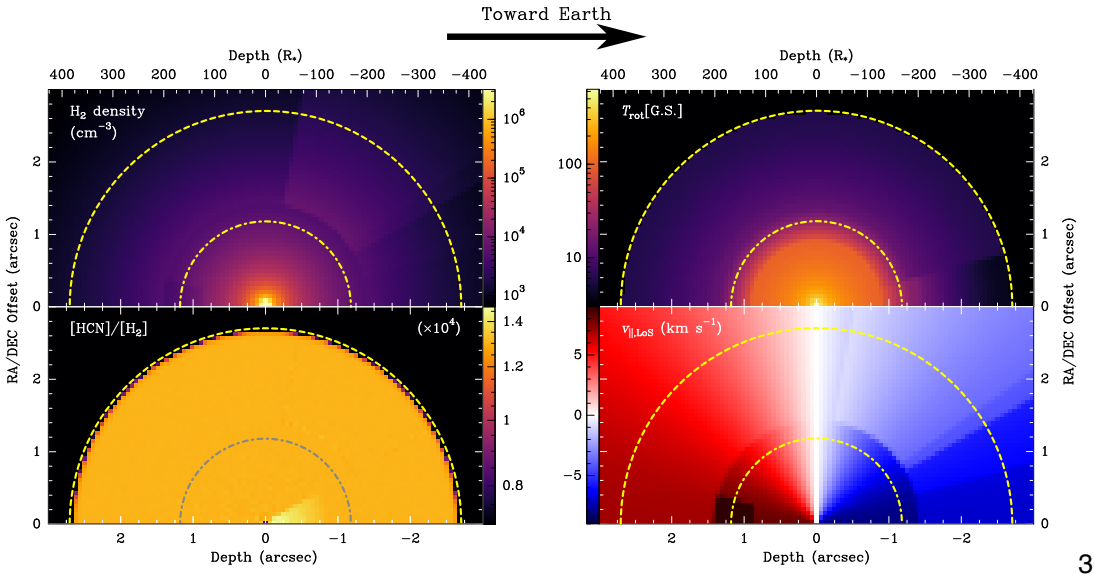

HCN in the C-rich star Y CVn: Conclusions

- Existence of asymmetries in the physical and chemical conditions at different distances from the star.
- The gas accelerates up to $\simeq 8$ km s^{-1} from the photosphere until $r \simeq 3R_\star$ beyond the photosphere. The terminal velocity ranges from 6 to 10 km s^{-1} but it can be even higher (possible tilted high velocity outflows).
- The lines in the mid-IR are broader than expected (elemental line widths of $\simeq 10$ km s^{-1} at the photosphere, which implies a turbulent velocity of $\simeq 6$ km s^{-1} or matter ejection mechanisms not considered in our models).
- HCN abundance with respect to H_2 $\lesssim 1.3 \times 10^{-4}$. It can be variable at the stellar photosphere. $N_{\rm col} \simeq 2.1 - 3.5 \times 10^{18}$ cm^{-2}, i.e., only one order of magnitude lower than for IRC+10216 but $\dot{M}_{\odot,\rm IRC+10216} \simeq 180 \dot{M}_{\odot,\rm Y\,CVn}$ ($\dot{M}_{\odot,\rm Y\,CVn} \simeq 1.5 \times 10^{-7}$ M$_\odot$ yr^{-1}).
- HCN is rotationally and vibrationally out of LTE throughout the whole envelope.
- Maser emission in $v = 0$ $J = 1 - 0$ and ν_2^{1e} $J = 3 - 2$. The ν_2^{1f} $J = 3 - 2$ can also be a weak maser.
- ^{12}C/^{13}C $\simeq 2.5$ (compatible with that of, e.g., Abia et al. 2017).
- Fonfría, Montiel, Cernicharo, DeWitt, Richter, et al., 2021, A&A, 651, A8

Final remarks

- The inner envelopes of low mass-loss rate AGB stars apparently contain complex structures related to matter ejection mechanisms and the molecular gas is highly excited.
- The comparison of these regions of the envelopes of high and low mass-loss rate stars can help us understand the evolution of the matter ejection process.
- High spectral resolution infrared observations complement interferometry in the description of the inner regions of circumstellar envelopes. It is not possible to obtain high spatial resolution maps from them but the ro-vibrational spectrum encodes the excitation conditions and gas kinematics.
- Column densities are more reliable when estimated from infrared observations as in the inner envelopes a significant fraction of the molecules, typically $30 - 70\,\%$, are vibrationally excited.
- SOFIA is a unique observatory to get infrared observations. Molecules abundant in the atmosphere, such as CO_2 or CH_4, are very difficult to be observed from the ground but they can be observed from the stratosphere. Telluric contamination is severely reduced when other molecules are observed.